Commun. Theor. Phys. **76** (2024) 085201 (12pp) https://doi.org/10.1088/1572-9494/ad4cdd

A study on vector mediator top-philic dark matter

Yanyan Hu[1], **Yandong Liu**[1,2,*] **and Yuanyuan Liu**[1,2]

[1] College of Nuclear Science and Technology, Beijing Normal University, Joint Laboratory of Jinping Ultra-low Radiation Background Measurement of Ministry of Ecology and Environment, Jinping Deep Underground Frontier Science and Dark Matter Key Laboratory of Sichuan Province, Key Laboratory of Beam Technology of Ministry of Education, Beijing 100875, China
[2] Beijing Radiation Center, Beijing 100875, China

E-mail: huyy@mail.bnu.edu.cn, ydliu@bnu.edu.cn and yyliu@bnu.edu.cn

Received 8 April 2024, revised 13 May 2024
Accepted for publication 17 May 2024
Published 5 July 2024

Abstract

We conducted a study on a simplified dark matter model that introduces a vector-like intermediate particle, facilitating exclusive interactions between dark matter and the top quark in the Standard Model. The analysis focused on the relic density of Dirac-type fermion dark matter and highlighted the complementary role of direct detection in constraining the dark matter model. Notably, in instances when dark matter mass is small, the tree-level two-body annihilation process experiences suppression. In such scenarios, the contributions of the three-body process ($\chi\bar{\chi} \to t\bar{b}W^-$) and the one-loop process ($\chi\bar{\chi} \to gg$) dominate the relic abundance. With regard to direct detection, calculations were performed for the two-loop contribution to the dark-matter–gluon interaction, yielding the corresponding spin-independent scattering cross section.

Keywords: dark matter, new physics, effective field theory

(Some figures may appear in colour only in the online journal)

1. Introduction

Dark matter (DM) remains one of the most enigmatic puzzles in the realm of particle physics and cosmology. Its existence, inferred from a multitude of astrophysical and cosmic scale observations, ranging from the rotation curves of galaxies and gravitational lensing to the precision measurements of the cosmic microwave background (CMB), highlights a significant void in our comprehension of the Universe's fundamental structure [1–4]. These observations provide compelling evidence of DM's gravitational influence; yet its precise particle physics properties continue to elude direct detection (DD). This presents not only a formidable challenge, but also an unprecedented opportunity for both theoretical and experimental physics to advance our understanding of particle physics.

Among the various candidates proposed to account for DM, the weakly interacting massive particles (WIMPs) stand out due to their compatibility with the relic density in the Universe [5–7]. WIMPs are theorized to have mass around the electroweak scale and engage in interactions at the weak interaction strength: characteristics that allow them to be thermally produced in the early universe via the freeze-out mechanism [8–10]. This process naturally results in a relic density that aligns with the CMB measurements, $\Omega_{\rm DM}h^2 = 0.1192 \pm 0.0010$ [11], making WIMPs a compelling candidate for DM. However, the quest for DD of WIMPs through observations of nucleon recoil from DM–nucleon scattering has so far yielded no conclusive results. This challenge is largely attributed to the cross-symmetry that links the DD process with the freeze-out mechanism, underscoring the complexities associated with the direct detection of DM.

The investigation of top-quark philic DM has emerged as a compelling avenue to address the discrepancies between the null results from DD experiments and the observed DM relic density. The absence of the top quark in nucleons introduces a natural suppression mechanism for DD processes. Concurrently, the top quark's designation as the heaviest particle in

* Author to whom any correspondence should be addressed.

the Standard Model (SM) and its essential role in electroweak symmetry breaking highlight its potential as a portal to DM [12, 13]. This paradigm has resulted in extensive research into the interaction dynamics of top-quark philic DM, aiming to evaluate its visibility through direct, indirect and collider search strategies. Such efforts represent a significant advancement in our quest to resolve DM, with DM models that interact with the top quark through high-dimensional operators posited for testing at the Large Hadron Collider (LHC) and in DM search experiments [14–17]. Models employing s-channel scalar mediators [18–20] or gauge boson mediators [21, 22] have been explored for collider implications. Additionally, numerous scalar DM models featuring a t-channel fermionic mediator have previously been examined [23–33].

The gauge boson mediator approach, particularly within the framework of $U(1)'$ extended models [34], introduces the Z' gauge boson as the mediator [35–38]. The $U(1)'$ gauge symmetry may arise from extensions of the SM gauge group [37], from unification models [39, 40] or from string theories [41, 42]. The gauge boson can acquire mass either through spontaneous symmetry breaking or via the Stueckelberg mechanism [43, 44]. For further details, see [34]. The top-quark philic model has been discussed in the context of DM [21], galactic gamma-ray lines [45, 46] and vacuum stability [47]. Simplified models of top-quark philic Z' have been studied in [48–50]. This Z' top-quark philic model has predominantly been investigated in the context of the LHC through top-quark pair association production [22, 48], single-top-quark associated production [51] or four top-quark productions [49–51]. With the associated production, the constraint on the Z' depends on both its coupling to the top quark and DM, namely the invisible decay branching ratio in the low-mass region. For instance, below the mass threshold for top-quark pair production, the coupling strength (g_t) is typically constrained to about 0.5. However, for a very low mass around 100 GeV, the constraints are more dependent on the specific model [22]. Additionally, the Z''s impact on electroweak precision measurements has been studied [22, 52, 53], indicating that, without mixing between $U(1)'$ and $U(1)_Y$, a lower bound of approximately 100 GeV is permitted for m_V/g_t. This limit varies, based on the details of the underlying theory and the degree of fine-tuning required.

In this work, we are dedicated to the DM narrative, with a focus on DD experiments. Adopting a general stance, we consider DM as a Dirac fermion interacting with the top quark via a gauge boson V. Our analysis of the DM relic density encompasses not only two-body processes, such as $\chi\bar{\chi} \to t\bar{t}$ and $\chi\bar{\chi} \to VV$, but also includes loop-generated processes $\chi\bar{\chi} \to gg$ and three-body processes $\chi\bar{\chi} \to t\bar{t}^*$, which become critical for low-mass DM particles χ. By examining the DM–nucleon scattering, we concentrate on the spin-independence interaction ($\bar{\chi}\chi G^a_{\mu\nu}G^{a\mu\nu}$), facilitated through two-loop corrections due to the top quark's absence in the nucleon.

The outline of this paper is as follows: in section 2 we set up the top-philic DM model, in which DM interacts with the SM via vector boson mediator particles. In section 3, the model is constrained by the cosmological determination of the correct relic density of DM, and the effects arising from the presence of new resonance states are summarized. In section 4, we calculate the $\sigma_{\rm SI}$ between DM and nucleons involving two-loop processes, obtaining the impact on DD constraints. We present our conclusion in section 5.

2. Model setup

In this study, we adopt a simplified model framework to investigate the interactions between the DM and the SM particles, facilitated by a new mediator. We introduce a Dirac fermion, χ, as the DM candidate, and an additional vector boson, V_μ, serving as the mediator. This vector boson V_μ could represent an extended $U(1)'$ gauge boson [34], engaging exclusively with the right-handed top quark [22]. The Lagrangian for our simplified model is expressed as follows:

$$\begin{aligned}\mathcal{L} \supset \mathcal{L}_{\rm SM} + \bar{\chi}(\mathrm{i}\partial\!\!\!/ - m_\chi)\chi + \frac{1}{2}V^\mu(-\Box - m_V^2)V_\mu \\ +\bar{\chi}(a_\chi + b_\chi\gamma_5)\gamma^\mu\chi V_\mu + g_t\bar{t}\gamma^\mu P_{\rm R}tV_\mu,\end{aligned} \tag{2.1}$$

where m_V and m_χ denote the masses of the vector boson V_μ and DM χ, respectively; $P_{\rm R}$ is a right-handed projector operator, which ensures the gauge boson V couples with the right-handed top quark uniquely; a_χ and b_χ represent the vector and axial-vector current couplings between V and χ, respectively; g_t represents the couplings between V and the top quark. To ensure the vector boson V_μ behaves as a narrow resonance, its total width must be less than about 10% of its mass m_V. We initially examine the decay width of the vector boson V_μ. The principal decay modes at tree level are $V \to t\bar{t}$ and $V \to \chi\bar{\chi}$, provided the energy threshold is met. The three-body decay modes, such as $V \to t\bar{t}^*$ ($t^*\bar{t}$), and the loop-induced decay modes, $V \to W^+W^-$ and $V \to Zh$, are considered negligible due to phase space and loop factor suppression. The partial decay widths of the tree-level processes $V \to t\bar{t}$ and $V \to \chi\bar{\chi}$ are given by:

$$\begin{aligned}\Gamma(V \to t\bar{t}) = \frac{3g_t^2\sqrt{m_V^2 - 4m_t^2}}{48\pi m_V^2}[(m_V^2 + 2m_t^2) \\ + (m_V^2 - 4m_t^2)]\Theta(m_V - 2m_t),\end{aligned} \tag{2.2}$$

$$\begin{aligned}\Gamma(V \to \chi\bar{\chi}) = \frac{\sqrt{m_V^2 - 4m_\chi^2}}{12\pi m_V^2}[a_\chi^2(m_V^2 + 2m_\chi^2) \\ + b_\chi^2(m_V^2 - 4m_\chi^2)]\Theta(m_V - 2m_\chi),\end{aligned} \tag{2.3}$$

where m_t represents the mass of the top quark, and $\Theta(x)$ denotes the Heaviside step function. The partial decay width of the V is displayed in figure 1. It is shown that the vector boson V is a narrow resonance for the parameter space of interest in the work. It is notable that the three-body decay

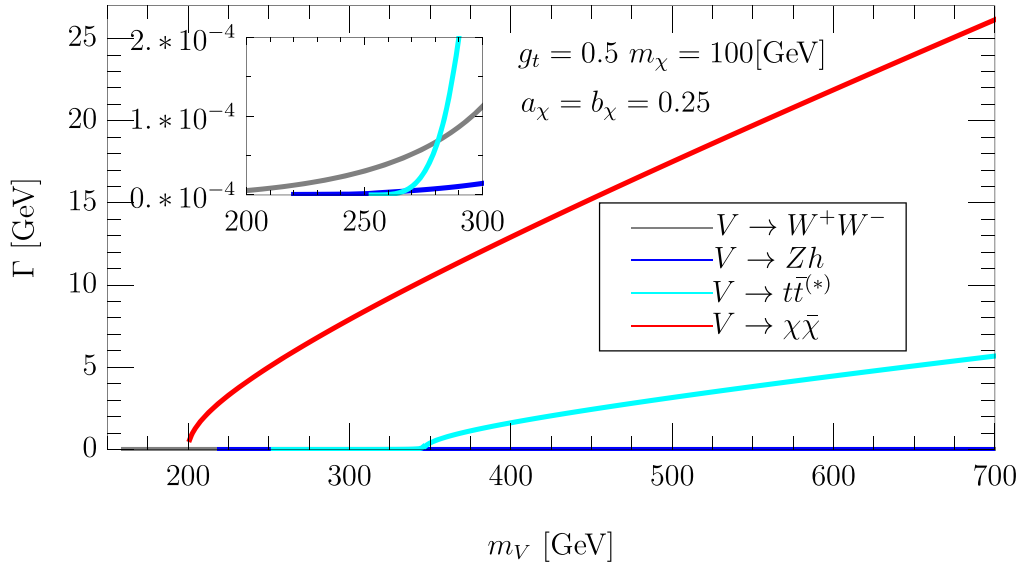

Figure 1. The partial decay width of the vector boson V as a function of the mass m_V and DM mass fixed to $m_\chi = 100$ GeV.

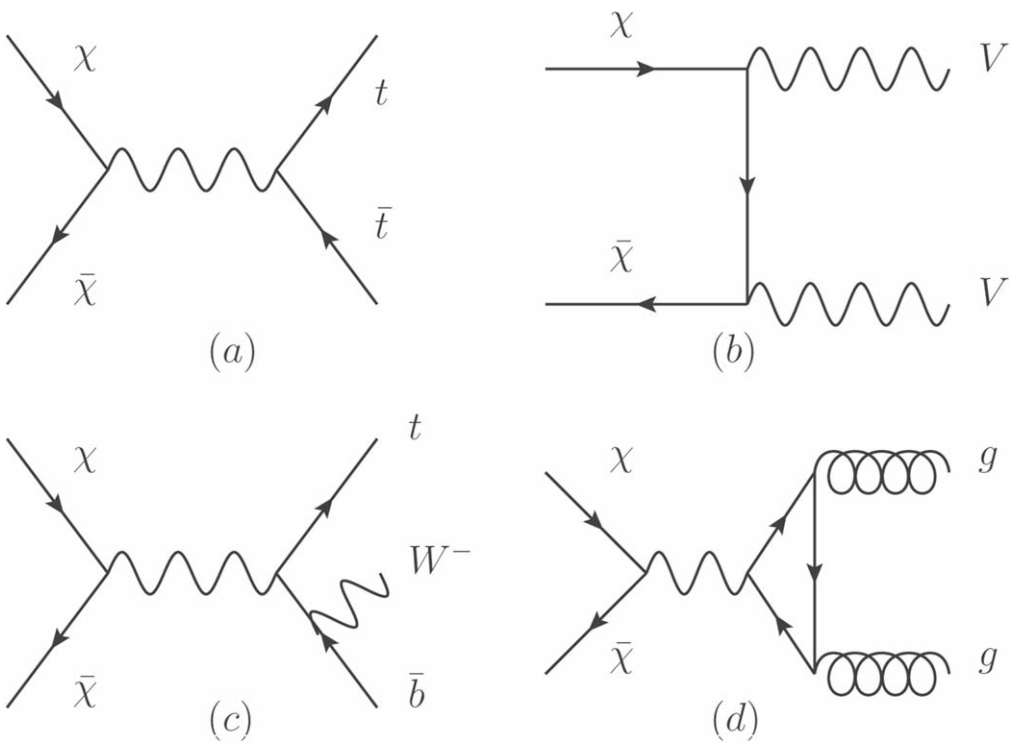

Figure 2. In this simplified model, DM annihilation involves tree-level two-body processes (a) and (b), a three-body process (c) and one-loop process (d), all contributing to DM relic abundance.

process $V \to t\bar{t}^*$ is dominant over the loop-induced processes when the vector boson mass is larger than about 250 GeV.

3. Dark matter relic abundance

The Planck satellite experiment has conducted high-precision measurement of DM relic abundance, yielding the result $\Omega_{\rm DM}h^2 = 0.1192 \pm 0.0010$. This measurement necessitates that the theoretical predictions for relic abundance in the simplified model should be lower than the observed value to prevent an excessive abundance of DM processes in the Universe. During the Universe's evolution, DM density can be calculated using the Boltzmann equation [7, 54]

$$\frac{{\rm d}Y}{{\rm d}x} = -\sqrt{\frac{\pi}{45}} m_{\rm PL} m_\chi \frac{g_{*s} g_*^{-1/2}}{x^2} \times \langle \sigma v_{\rm rel} \rangle [Y^2 - (Y^{\rm EQ})^2], \tag{3.1}$$

and its relic abundance is given by

$$\Omega_\chi h^2 \approx 2.76 \times 10^8 Y \frac{m_\chi}{\mathrm{GeV}}, \tag{3.2}$$

where Y is the DM number density of today in a comoving reference frame

$$Y = \sqrt{\frac{45}{\pi}} \frac{g_*(x_f)^{1/2}/g_{*s}(x_f)}{m_{\mathrm{PL}} m_\chi \langle \sigma v_{\mathrm{rel}} \rangle} x_f. \tag{3.3}$$

Here, $x_f \equiv m_\chi/T_f$, where T_f corresponds to the DM decoupling temperature and $m_{\mathrm{PL}} = 1.22 \times 10^{19}$ GeV corresponds to Planck mass. The $g_*(x_f)$ and $g_{*s}(x_f)$ correspond to the effective and entropic degrees of freedom at the DM decoupling temperature, respectively. Thus, the annihilation cross section $\langle \sigma v_{\mathrm{rel}} \rangle$ corresponds to,

$$\langle \sigma v_{\mathrm{rel}} \rangle \approx 0.71 \frac{0.12}{\Omega_\chi h^2} \frac{x_f}{25} \frac{g_*(x_f)^{1/2}/g_{*s}(x_f)}{0.1} \text{ pb}. \tag{3.4}$$

The annihilation cross section can be expanded in small amounts, depending on the velocity, i.e. $\langle \sigma v_{\mathrm{rel}} \rangle = a + b\langle v_{\mathrm{rel}}^2 \rangle + \mathcal{O}(\langle v_{\mathrm{rel}}^4 \rangle)$. The coefficients a and b correspond to the contributions of s-wave and p-wave scattering, respectively.

In the simplified model, DM pairs can annihilate into various final states, such as $\bar{t}t$, VV, gg and $t\bar{b}W^-$, depending on the properties of the involved particles [55–59]. For DM mass exceeding that of the top quark, χ can annihilate into a pair of top quarks via a resonance-mediated s-channel process. The thermally averaged cross section for this process is approximated as:

$$\langle \sigma v_{\mathrm{rel}} \rangle_{\chi\bar{\chi}\to t\bar{t}} \simeq \frac{3 g_t^2 \beta_t [2 a_\chi^2 \beta_t^2 m_\chi^2 + a_\chi^2 (m_t^2 + 2 m_\chi^2) + (b_\chi \beta_\chi^2 m_t)^2]}{8\pi (\beta_\chi m_V)^4}, \tag{3.5}$$

where $\beta_t = \sqrt{1 - m_t^2/m_\chi^2}$ and $\beta_\chi = \sqrt{1 - 4m_\chi^2/m_V^2}$ denote the velocities of the top quark and the DM, respectively. If $m_\chi > m_V$, DM can also annihilate into a pair of vector bosons, with the thermally averaged cross section given by:

$$\langle \sigma v_{\mathrm{rel}} \rangle_{\chi\bar{\chi}\to VV} \simeq \frac{\beta_V^3 [(a_\chi^4 + b_\chi^4) m_V^2 + 2 a_\chi^2 b_\chi^2 (4 m_\chi^2 - 3 m_V^2)]}{4\pi m_\chi^2 m_V^2 (2 - m_V^2/m_\chi^2)^2}, \tag{3.6}$$

with $\beta_V = \sqrt{1 - m_V^2/m_\chi^2}$ representing the velocity of the vector boson. Several points warrant emphasis regarding the above thermally averaged cross sections:

- Equations (3.5) and (3.6) primarily showcase s-wave contributions. Nevertheless, in a detailed analysis, both s-wave and p-wave components are crucial, given $\langle v_{\mathrm{rel}}^2 \rangle \sim 0.3$ during DM decoupling.
- The $\chi\bar{\chi} \to t\bar{t}$ process, being s-channel, exhibits Breit–Wigner enhancement, especially when $m_\chi \simeq m_V/2$. This effect is evident from the $1/\beta_\chi^4$ term in equation (3.5).

For scenarios where $m_\chi < m_t$, three-body decay processes like $\bar{\chi}\chi \to t\bar{b}W^-$ and loop-induced processes such as $\bar{\chi}\chi \to gg$ become dominant in DM annihilation [60–62], surpassing $\chi\bar{\chi} \to t\bar{t}$. The thermally averaged cross section for $\bar{\chi}\chi \to gg$ is expressed as:

$$\langle \sigma v_{\mathrm{rel}} \rangle_{\chi\bar{\chi}\to gg} \simeq \frac{\alpha_s^2 g_t^2 b_\chi^2 m_\chi^2 (N_c^2 - 1)}{64\pi^2 m_V^4} \times \left| \frac{\tau}{4} \ln^2 \left[\frac{2\sqrt{1-\tau} + \tau - 2}{\tau} \right] + 1 \right|^2, \tag{3.7}$$

where $\tau = 4m_t^2/q^2$. It is clearly shown that the cross section only depends on the axial current interaction as it is generated from the axial anomaly. Notably, no Breit–Wigner enhancement is observed in this process, a consequence of the on-shell V process being forbidden by the Landau–Yang Theorem. It provides a detailed comparison between two DM annihilation processes in [15]. And it demonstrates that the loop-induced process $\chi\bar{\chi} \to gg$ predominates when the DM mass, m_χ, is below approximately 130 GeV. Conversely, when m_χ exceeds 130 GeV, the three-body process $\chi\bar{\chi} \to t\bar{b}W^-$ becomes the dominant mechanism influencing the DM relic abundance.

In the following, we present our numerical results regarding the DM relic density. Using detailed computational analysis, we identify regions of parameter space that are consistent with the Planck satellite's measurement of the DM relic density, specifically focusing on the interplay between the coupling constants a_χ, b_χ and the DM mass m_χ in figures 3 and 4. In figure 3, we delineate the parameter space (cyan shaded region) that aligns with the Planck satellite observations. This figure concentrates on the lower DM mass range, where two-body decay processes are kinematically forbidden. It is observed that, compared to loop-induced processes, the three-body process predominantly governs the parameter space. However, at a lower DM mass of approximately 150 GeV and a substantial coupling $g_t = 0.5$, the loop contribution from the process $\chi\bar{\chi} \to gg$ becomes non-negligible. Figure 4 explores the DM relic density in the higher-mass regime, with the red line indicating the threshold $\Omega_\chi h^2 = 0.1198$. Notably, a Breit–Wigner enhancement is evident around $m_\chi \simeq m_V/2$, which allows for smaller couplings of g_t to suffice; this effect is visibly represented as a valley in the red line. In the subplot of figure 4(b), we note a decrease in the couplings a_χ and b_χ as m_χ exceeds m_V, signifying the pivotal role of the $\chi\bar{\chi} \to VV$ process in the evolution of DM, especially when $a_\chi = b_\chi \approx 0.5$. It is important to note the presence of a threshold effect in the right subplot when the DM mass exceeds the vector boson mass m_V, an effect that is absent in the left subplot. This distinction arises because the annihilation mode $\chi\bar{\chi} \to VV$ predominates in the relic density calculation in the right plot, facilitated by the couplings $g_t = 0.2$ in comparison to $a_\chi = b_\chi \approx 0.5$. Conversely, in the left plot, the contribution from this mode is negligible relative to $\chi\bar{\chi} \to V \to t\bar{t}$, due to the stronger coupling $g_t = 0.5$ and weaker $a_\chi = b_\chi \approx 0.2$.

Further analysis is presented in figure 5, which maps the DM relic density against the plane of m_V and m_χ for fixed couplings, focusing respectively on low and high DM mass

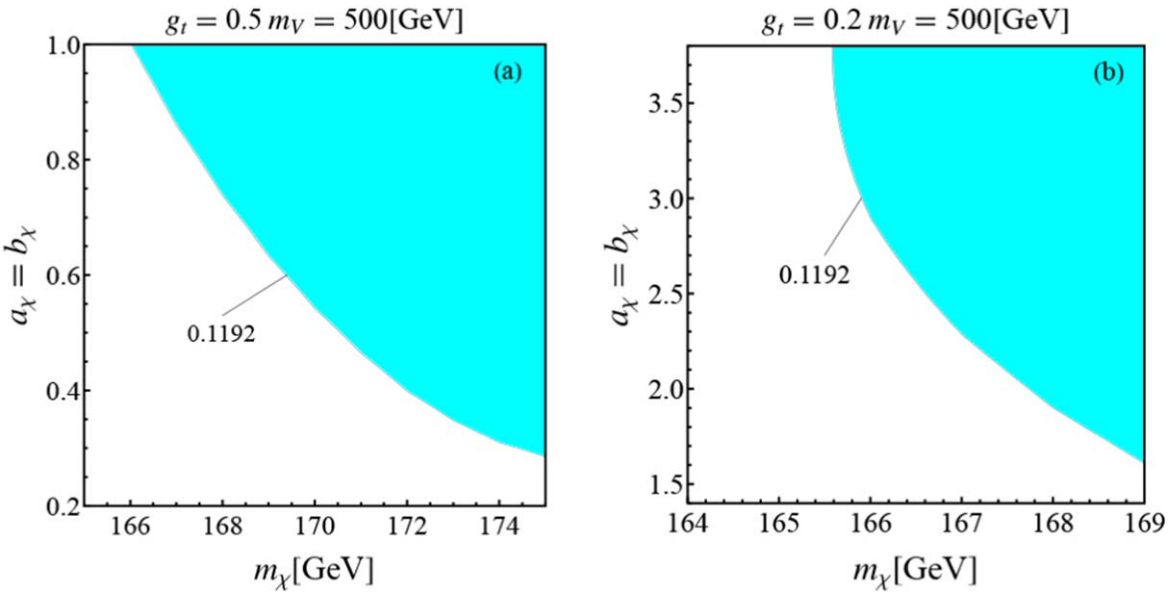

Figure 3. The relic density of DM χ plotted in the plane of coupling a_χ (b_χ) versus mass m_χ, with the vector boson mass m_V and its couplings to the top quark g_t held constant. Subgraphs (a) and (b) show the numerical results for $g_t = 0.5$ and $g_t = 0.2$, respectively. The colored region indicates the parameter space that accommodates a relic density $\Omega_\chi h^2 \leqslant 0.1192$. Notably, the mass of the DM m_χ is considered to be less than that of the top quark.

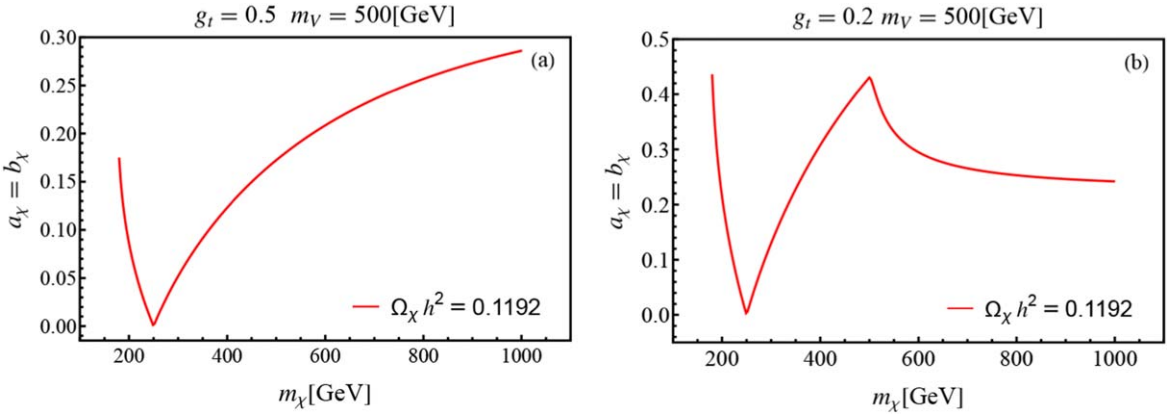

Figure 4. The relic density of DM χ, illustrated in the plane of coupling a_χ (b_χ) versus mass m_χ, with the mass of the vector boson m_V and its coupling to the top quark g_t maintained constant. Subgraphs (a) and (b) show the numerical results for $g_t = 0.5$ and $g_t = 0.2$, respectively. The red line delineates $\Omega_\chi h^2 = 0.1192$, and the DM mass m_χ is considered to be larger than top-quark mass.

regions. The cyan regions in these figures correspond to parameter spaces fulfilling the current measuring of DM relic abundance. Specifically, figures 5(a) and (b) employ two distinct sets of coupling constants: $g_t = 0.2\,(0.5)$, and $a_\chi = b_\chi = 0.1(0.25)$. In the domain of lower m_χ, the significance of the three-body process is underscored, with resonance enhancement near $2m_\chi \sim m_V$ contributing to the achievement of the correct relic abundance. Conversely, figure 5 demonstrates that, in the regime of larger DM mass, two-body annihilation processes become dominant. With smaller couplings, as shown in figure 5(c), resonance enhancement is crucial for maintaining the DM relic density requirements, with the permissible parameter space concentrated around $m_\chi \sim m_V/2$. With larger couplings, as illustrated in figure 5(d), besides the enlarged parameter space around $m_\chi \sim m_V/2$, an additional parameter space for $m_\chi > m_V$ is also viable, due to the contribution from the $\chi\bar{\chi} \to VV$ process.

4. Dark matter direct detection

The DD experiments are one of the foundational approaches in the search for DM. The goal is to directly observe the rare scattering events between the non-relativistic DM particles and the target material. These scattering cross sections can be further categorized into spin-independent (SI) and spin-dependent (SD) contributions [63–68], reflecting the nature of the interaction between DM and the target nuclei. Since SI scattering interacts coherently with the entire nucleus, the cross section with respect to the target nucleon can be

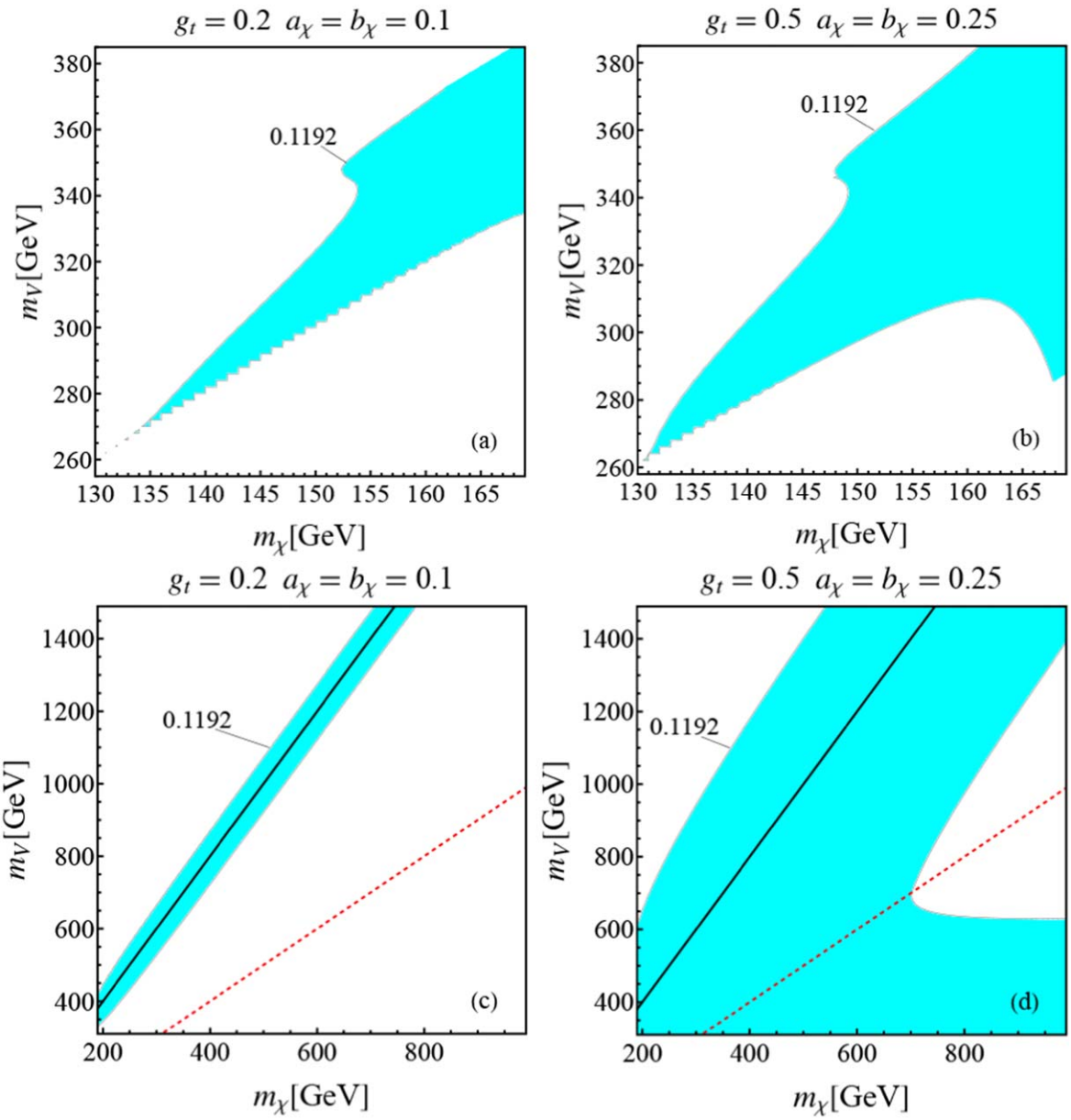

Figure 5. The relic density of DM χ displayed in the plane of vector boson mass m_V and m_χ with constant couplings g_t, a_χ, b_χ. The colored region denotes the parameter space with $\Omega_\chi h^2 \leqslant 0.1192$. Subgraphs (a) and (b) correspond to smaller DM and intermediate mass, and subgraphs (c) and (d) correspond to larger DM mass and intermediate mass. In (c) and (d), the black line indicates the condition $2m_\chi \approx m_V$, near which resonance enhancement is observed; the red dotted line marks the condition $m_\chi \approx m_V$.

succinctly expressed as

$$\sigma^{\rm SI} = \frac{4\mu_\chi^2}{\pi} A^2 \lambda_N^2, \tag{4.1}$$

which scales with the squared number of scattering centers (nucleons). Here, A is the atomic mass number of the target nuclei; μ_χ is the reduced mass of the DM–nucleon, defined as $\mu_\chi = \frac{m_\chi m_N}{(m_\chi + m_N)}$, and we treat m_N as the mass of protons. The λ_N are the coupling constants of DM with the nucleon, defined as

$$\lambda_{p(n)} = m_N \sum_{q=u,d,s} \left(f_q f_{Tq} + \frac{3}{4}(q(2) + \bar{q}(2))(g_q^{(1)} + g_q^{(2)}) \right) - \frac{8\pi}{9\alpha_s} f_{TG} f_G + \frac{3}{4} G(2)(g_G^{(1)} + g_G^{(2)}),$$

where f_{Tq}, f_{TG}, $q(2)$, $\bar{q}(2)$ and $G(2)$ are hadronic matrix elements [69, 70]

$$m_f f_{Tq} = \langle N | m_q \bar{q} q | N \rangle \quad f_{TG} \equiv 1 - \sum_{u,d,s} f_{Tq},$$
$$\langle N(p) | \mathcal{O}^q_{\mu\nu} | N(p) \rangle = \frac{1}{m_{\rm N}} \left(p_\mu p_\nu - \frac{1}{4} m_{\rm N}^2 g_{\mu\nu} (q(2) + \bar{q}(2)) \right),$$
$$\langle N(p) | \mathcal{O}^g_{\mu\nu} | N(p) \rangle = \frac{1}{m_{\rm N}} \left(p_\mu p_\nu - \frac{1}{4} m_{\rm N}^2 g_{\mu\nu} G(2) \right), \tag{4.2}$$

where $m_{\rm N}$ is the nucleon mass and N is the proton or neutron. The values of hadronic matrix elements are given by [69]

$$f_{Tu}^p = 0.018, \quad f_{Td}^p = 0.030, \quad f_{Tu}^n = 0.015,$$
$$f_{Td}^n = 0.034, \quad f_{TG} = 0.80, \tag{4.3}$$

where f_{Tq}^{N} corresponds to the contribution of the quark q to the nucleon matrix elements for the nucleon N. The matrix elements of the twist-2 operators are related to the second moments of the parton distribution functions (PDFs),

$$q(2)+\bar{q}(2)=\int_0^1 \mathrm{d}x x(q(x)+\bar{q}(x)),$$
$$G(2)=\int_0^1 \mathrm{d}x x g(x), \tag{4.4}$$

where $q(x)$, $\bar{q}(x)$ and $g(x)$ are the PDFs of the quark, anti-quark and gluon in nucleon N, respectively. Those hadronic elements could be extracted from the CT14NNLO PDFs [70],

$$[u(2)+\bar{u}(2)]_p=0.3481,\quad [d(2)+\bar{d}(2)]_p=0.1902,$$
$$G(2)_p=G(2)_n=0.4159. \tag{4.5}$$

The f_q, f_G, $g_q^{(1)}$, $g_q^{(2)}$, $g_G^{(1)}$ and $g_G^{(2)}$ are Wilson coefficients of corresponding operators which describe the SI scattering. The effective Lagrangian [71, 72] exhibits as

$$\mathcal{L}=\sum_{u,d,s}\mathcal{L}_q^{\mathrm{EFT}}+\mathcal{L}_g^{\mathrm{EFT}}, \tag{4.6}$$

where

$$\mathcal{L}_q^{\mathrm{EFT}}=f_q m_q\bar{\chi}\chi\bar{q}q+\frac{g_q^{(1)}}{2m_\chi}\bar{\chi}i(\partial^\mu\gamma^\nu+\partial^\nu\gamma^\mu)\chi O_{q,\mu\nu}^{(2)}$$
$$+\frac{g_q^{(2)}}{m_\chi^2}\bar{\chi}(i\partial^\mu)(i\partial^\nu)\chi O_{q,\mu\nu}^{(2)}, \tag{4.7}$$

$$\mathcal{L}_g^{\mathrm{EFT}}=f_G\,\bar{\chi}\chi G^a_{\mu\nu}G^{a\mu\nu}+\frac{g_G^{(1)}}{2m_\chi}\bar{\chi}i(\partial^\mu\gamma^\nu+\partial^\nu\gamma^\mu)\chi O_{G,\mu\nu}^{(2)}$$
$$+\frac{g_G^{(2)}}{m_\chi^2}\bar{\chi}(i\partial^\mu)(i\partial^\nu)\chi O_{G,\mu\nu}^{(2)}. \tag{4.8}$$

The twist-2 operators $O_{q,\mu\nu}^{(2)}$ and $O_{G,\mu\nu}^{(2)}$ are defined as

$$O_{q,\mu\nu}^{(2)}\equiv\frac{1}{2}\bar{q}(\gamma^{\{\mu}\,iD_-^{\nu\}}-\frac{g^{\mu\nu}}{4}i\not{D}), \tag{4.9}$$
$$O_{G,\mu\nu}^{(2)}\equiv -G^{a\mu\lambda}G^{a\nu}_{\ \ \lambda}+\frac{g^{\mu\nu}}{4}(G^a_{\alpha\beta})^2. \tag{4.10}$$

Here, f_q, f_G, $g_q^{(1)}$, $g_q^{(2)}$, $g_G^{(1)}$ and $g_G^{(2)}$ could match to our simplified model.

In the simplified model, the vector boson mediator uniquely interacts with the top quark in the SM; therefore, we focus on the DM–nucleon scattering induced from the operator $\bar{\chi}\chi G^a_{\mu\nu}G^{a\mu\nu}$ as the twist-2 operator denotes high-order effects. The operator is generated at the loop level in the simplified model. The one-loop contribution from the cross one of the DM annihilation process $\chi\bar{\chi}\to gg$ is highly suppressed and negligible. It is attributed from this that the mediator vector boson is on-shell for the non-relativistic DM scattering at the leading order and the process is forbidden by the Landau–Yang theorem. The leading-order contribution comes from the two-loop Feynman diagrams, see figure 6. The matching coefficients f_G can be calculated using the usual method with the help of the projection operators. Alternatively, one can also use the Fock–Schwinger gauge to simplify the calculation [71, 73], i.e. $x^\mu A_\mu=0$. In this work, we will focus on the Fock–Schwinger gauge method and refer the reader to [74] for details of the projection operator approach. In the Fock–Schwinger gauge, one can express the gluon field in terms of its field strength tensor $G_{\mu\nu}$ and maintain explicit gauge invariance for each step in the calculation. The Wilson coefficients can be extracted from the two-loop correction, and it shows

$$f_G=\int\frac{\mathrm{d}^4p}{(2\pi)^4}[(a_\chi+b_\chi\gamma_5)\gamma^\alpha[(\not{p}_\chi-\not{p})+m_\chi]$$
$$\times(a_\chi+b_\chi\gamma_5)\gamma^\beta]$$
$$\times\frac{\left[g_{\alpha\mu}-\frac{p_\alpha p_\mu}{m_V^2}\right]\left[g_{\beta\nu}-\frac{p_\beta p_\nu}{m_V^2}\right]}{(p^2-m_V^2)(p^2-m_V^2)[(p_\chi-p)^2-m_\chi^2]}\mathcal{M}^{\mu\nu}(p), \tag{4.11}$$

in the limit of zero momentum transfer, where p_χ is the DM momentum and $\mathcal{M}^{\mu\nu}(p)$ denotes the top-quark box diagram contribution in figure 7. Using the Fock–Schwinger gauge it is obtained

$$\mathcal{M}^{\mu\nu}=\int_0^1\mathrm{d}x\left[\frac{ig_s^2g_t^2(4x^2(x-1)^2p^\mu p^\nu-m_t^2((8x^2-8x+3)-)g^{\mu\nu})}{192\pi^2\Delta^2}\right.$$
$$\left.+\frac{ig_s^2g_t^2m_t^2(m_t^2((2x^2-2x+1)+(1-2x)^2)g^{\mu\nu}-4(3x^3-6x^2+4x-1)p^\mu p^\nu)}{96\pi^2\Delta^3}+\frac{ig_s^2g_t^2x(1-x)g^{\mu\nu}}{48\pi^2\Delta}\right], \tag{4.12}$$

where $\Delta=x(x-1)p^2+m_t^2$. After integration, the Wilson coefficient of the gluon field can be expressed as

$$f_G=f_1A_0(m_V^2)+f_2A_0(m_t'^2)+f_3B_0(0,m_t'^2,m_t'^2)$$
$$+f_4B_0(0,m_V^2,m_V^2)+f_5B_0(m_\chi^2,m_\chi^2,m_t'^2)$$
$$+f_6B_0(m_\chi^2,m_V^2,m_\chi^2)$$
$$+f_7D_0(0,0,m_\chi^2,m_\chi^2,0,m_\chi^2,m_t'^2,m_t'^2,m_t'^2,m_\chi^2)$$
$$+f_8C_0(0,m_\chi^2,m_\chi^2,m_V^2,m_V^2,m_\chi^2)$$
$$+f_9C_0(0,m_\chi^2,m_\chi^2,m_t'^2,m_t'^2,m_\chi^2)$$
$$+f_{10}C_0(0,0,0,m_t'^2,m_t'^2,m_t'^2), \tag{4.13}$$

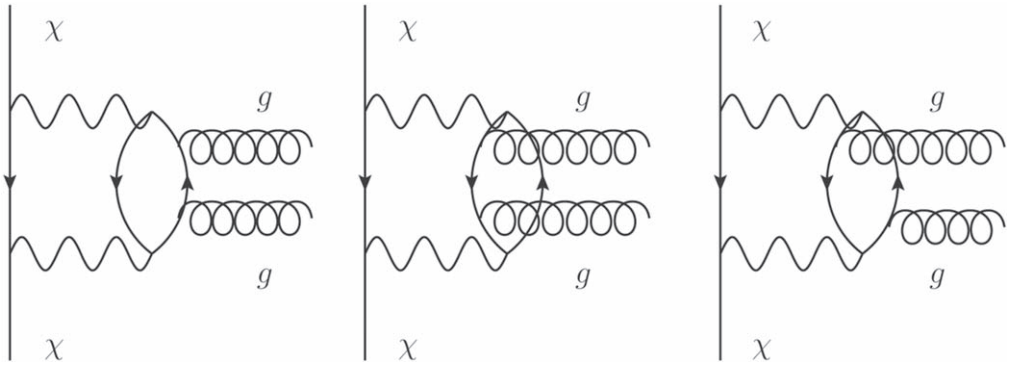

Figure 6. Two-loop Feynman diagrams depicting DM χ scattering with gluons.

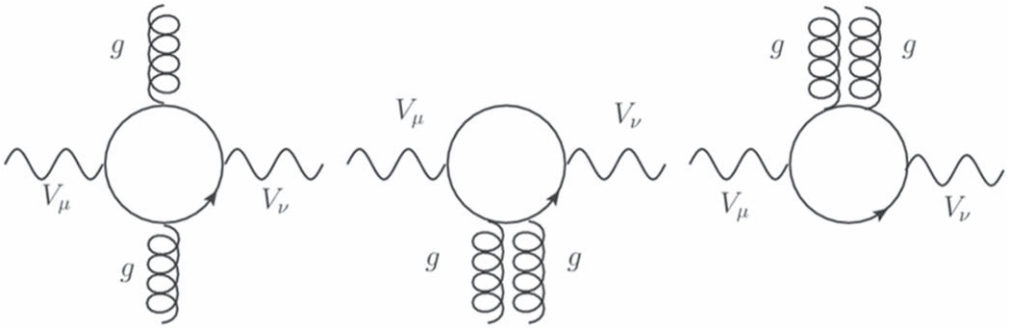

Figure 7. The box diagrams generating vector boson V scattering with gluons.

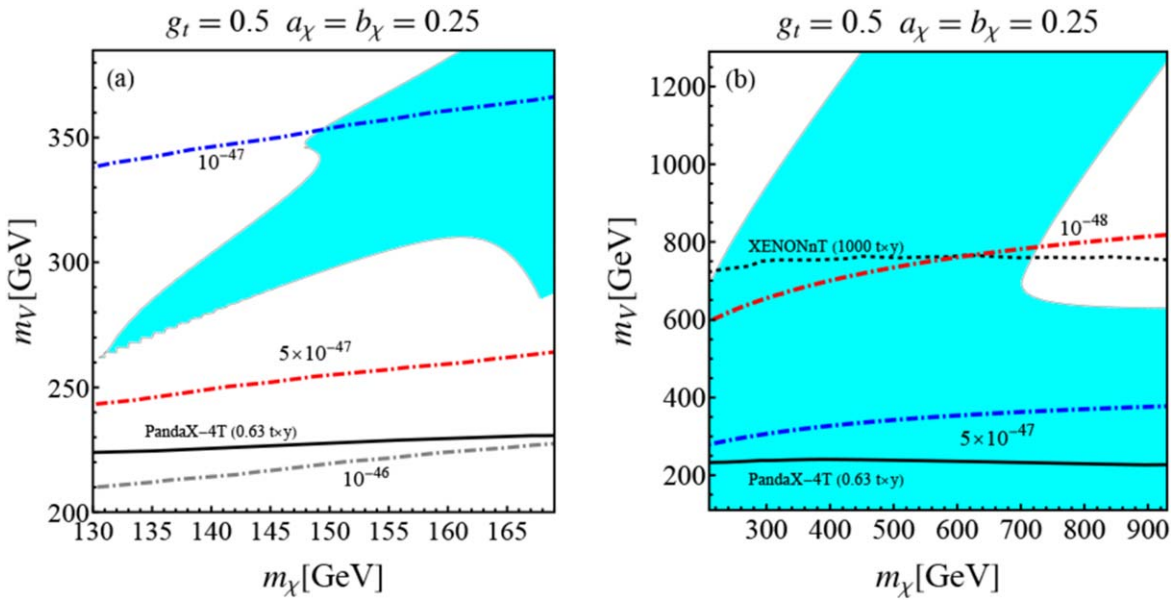

Figure 8. The DM–nucleon SI scattering cross section $\sigma^{\rm SI}_{\chi N}$ in the m_V and m_χ plane is illustrated. Subgraphs (a) and (b) correspond to numerical results for smaller/larger masses of DM and intermediate state, respectively. The colored dot–dashed lines indicate the contours of the cross sections. The solid and dashed black lines represent the results from the current DM DD experiment PandaX-4T (0.63 t×y) [77] and the projections for the future experiment XENONnT (1000 t×y) [78], respectively, with varying m_χ.

where $m_t' = \frac{m_t}{\sqrt{x(1-x)}}$, A_0, B_0, C_0 and D_0 are Passarino–Veltman scalar functions [75, 76]. The forms of f_1 to f_{10} are given in the appendix.

Next, we perform the numeric results on the DM–nucleon SI cross section, namely

$$\sigma^{\rm SI}_{\chi N} = \frac{256\pi\mu_\chi^2 m_{\rm N}^2}{81\alpha_s^2} f_{TG}^2 f_G^2, \tag{4.14}$$

in comparison DM DD experiments. In figure 8, we illustrate the predicted cross sections for a simplified model with the parameters set at $g_t = 0.5$ and $a_\chi = b_\chi = 0.25$. The contours of the SI scattering cross section ($\sigma^{\rm SI}_{\chi N}$) are depicted with solid lines in blue, pink and gray. The current experimental PandaX-4T (0.63 t×y) [77] limits on $\sigma^{\rm SI}_{\chi N}$ for varying DM masses are shown by the solid black line, while future projections (XENOTnT(1000 t × y))[78] are represented by the dashed

black line. Figure 8(a) presents the case where the DM mass (m_χ) is less than the mass of the top quark. In this scenario, the SI scattering cross section between DM and nucleons typically ranges from 10^{-47} to 10^{-46} cm^2. The current experimental limit on $\sigma^{\rm SI}_{\chi N}$ is about 10^{-46} cm^2 for low-mass DM, indicating that this range remains largely unconstrained. However, future projections suggest that all of this parameter space could be explored in upcoming DM DD experiments. Figure 8(b) addresses the scenario where the DM mass exceeds the top-quark mass, enabling the annihilation process $\chi\bar{\chi} \to t\bar{t}$. Here, $\sigma^{\rm SI}_{\chi N}$ values range between 10^{-47} and 10^{-48} cm^2, with portions already excluded by current DD experiments, as depicted by the solid black line. Particularly, the parameter space with vector boson masses below 200 GeV is inconsistent with current DD results. Future experiments are expected to probe the vector boson mass below 600 GeV, potentially testing much of the remaining parameter space.

5. Conclusions

In this study, we concentrate on a specific category of simplified DM models characterized by exclusive interactions with the top quark. We introduce a Dirac-type DM particle, denoted as χ, and a vector-like intermediate particle, V, into the simplified model. The model incorporates a comprehensive interaction schema that includes both vector and axial-vector couplings to DM. We proceed to derive the DM relic density, accounting for contributions from three-body processes and loop-induced mechanisms, which are crucial for modeling low-mass DM scenarios. Subsequently, we calculate the SI DM–nucleon cross section, which arises from two-loop interactions, denoted as $\bar{\chi}\chi GG$.

In the low DM mass region, the resonance effect is necessary to achieve the DM relic abundance, even with large couplings ($g_t \approx 0.5$ and $a_\chi \approx b_\chi \approx 0.25$). In this regime, the three-body annihilation process $\chi\bar{\chi} \to t\bar{b}W^-$ predominates in the early Universe. Conversely, for DM with a larger mass, the two-body annihilation processes $\chi\bar{\chi} \to VV$ and $\chi\bar{\chi} \to t\bar{t}$ are dominant in determining the DM relic abundance. In DM DD experiments, the parameter space for low-mass DM will be probed in future experiments (XENOTnT (1000 t × y)) with moderate couplings ($g_t \approx 0.5$ and $a_\chi \approx b_\chi \approx 0.25$) [78]. For cases where $m_\chi > 200$ GeV, the parameter space has already been excluded by current experiments (PandaX-4T (0.63 t×y)) if the vector boson mass is below 200 GeV [77]. In future experiments, the parameter space will be testable if the vector boson mass is less than approximately 600 GeV.

Acknowledgments

We would like to thank Shuangshuang Hu for her valuable discussions. The work is supported in part by the National Science Foundation of China under Grant Nos. 12222502 and 12075257.

Appendix

A.1. Integral formula

$$\frac{1}{AB} = \int_0^1 {\rm d}x \frac{1}{[xA + (1-x)B]^2}, \tag{A1}$$

$$\frac{1}{A^4B} = \int_0^1 {\rm d}x \frac{4x^3}{[xA + (1-x)B]^5}, \tag{A2}$$

$$\frac{1}{AB^4} = \int_0^1 {\rm d}x \frac{4(1-x)^3}{[xA + (1-x)B]^5}, \tag{A3}$$

$$\frac{1}{A^2B^2} = \int_0^1 {\rm d}x \frac{6x(1-x)}{[xA + (1-x)B]^4}. \tag{A4}$$

A.2. f_n

The functions $f_1 \sim f_{10}$, which are used in equation (4.13), are defined as

$$\begin{aligned} f_1 = {} & \frac{g_s^2(a_\chi^2 + b_\chi^2)}{24m_\chi x(x-1)(m_t'^2 - m_V^2)^4} \\ & \times [a_\chi^2(3m_t'^4 x(x-1) + m_t'^2 m_V^2 \\ & \times (10x - 10x^2 - 3) + m_V^4 x(x-1)) \\ & - b_\chi^2(m_t'^4(-11x^2 + 11x - 4) + m_t'^2 m_V^2 \\ & \times (-2x^2 + 2x + 1) + m_V^4 x(x-1))], \end{aligned} \tag{A5}$$

$$\begin{aligned} f_2 = {} & \frac{g_s^2(a_\chi^2 + b_\chi^2)}{24m_\chi x(x-1)(m_t'^2 - m_V^2)^4} \\ & \times [a_\chi^2(-3m_t'^4 x(x-1) + m_t'^2 m_V^2 \\ & \times (10x - 10x^2 - 3) - m_V^4 x(x-1)) \\ & + b_\chi^2(m_t'^4(11x^2 - 11x + 4) + m_t'^2 m_V^2 \\ & \times (2x^2 - 2x - 1) - m_V^4 x(x-1))], \end{aligned} \tag{A6}$$

$$\begin{aligned} f_3 = {} & \frac{g_s^2 g_t^2}{192m_\chi x(x-1)(m_t'^2 - m_V^2)^3} \\ & \times [(m_t'^2 + m_V^2(8x^2 - 8x + 3)) \\ & + (m_t'^2(16x^2 - 16x + 5) - m_V^2)], \end{aligned} \tag{A7}$$

$$\begin{aligned} f_4 = {} & \frac{g_s^2 g_t^2}{192m_\chi x(x-1)(m_t'^2 - m_V^2)^3} \\ & \times [(m_t'^4(6x^2 - 6x + 1) - 3m_t'^2 m_V^2(1-2x)^2 \\ & + 2m_V^2 x(x-1)) \\ & - (3m_t'^2 - m_V^2)(m_t'^2(2x^2 - 2x + 1) + 2m_V^2 x(x-1))], \end{aligned} \tag{A8}$$

$$
\begin{aligned}
f_5 = -f_6 = {} & \frac{g_s^2 g_t^2}{192 m_\chi x(x-1)(m_t'^2 - m_V^2)^4} \\
& \times[(b_\chi^2(m_t'^6(6x^2-6x+1) - 4m_t'^2 \\
& \times(m_V^2(3x^2-3x+1) + 2m_\chi^2(8x^2-8x+1)) \\
& + m_t'^2 m_V^2(m_V^2(-6x^2+6x-3) + 4m_\chi \\
& \times(18x^2-18x+5)) - 8m_V^4 m_\chi^2 x(x-1)) \\
& + b_\chi^2(m_t'^6(6x^2-6x+1) - 4m_t'^4 \\
& \times(m_V^2(3x^2-3x+1) - 3m_\chi^2 x(x-1)) \\
& - m_t'^2 m_V^2(m_V^2(6x^2-6x+3) + 4m_\chi^2 \\
& \times(10x^2-10x+3)) + 4m_\chi^4 m_\chi^2 x(x-1))) \\
& + (b_\chi^2(m_t'^6(-6x^2+6x+3) - 4m_t'^2 \\
& \times(m_V^2(5x^2-5x+1) - 2m_\chi^2(13x^2-13x+5)) \\
& + m_t'^2 m_V^2(m_V^2(2x^2+2x-1) - 4m_\chi(6x^2-6x+7) \\
& - 8m_V^4 m_\chi^2 x(x-1)) \\
& + a_\chi^2(m_t'^6(-6x^2+6x-3) - 4m_t'^4 \\
& \times(m_V^2(5x^2-5x+1) + m_\chi^2(11x^2-11x+4)) \\
& + m_t'^2 m_V^2(m_V^2(2x^2-2x+1) + 4m_\chi^2 \\
& \times(-2x^2+2x+1)) + 4m_\chi^4 m_\chi^2 x(x-1)))],
\end{aligned}
\tag{A9}
$$

$$
\begin{aligned}
f_7 = {} & \frac{g_s^2 g_t^2 m_t'^2}{96 m_\chi x(x-1)(m_t'^2 - m_V^2)^2} \\
& \times[(a_\chi^2(m_t'^2(2x^2-2x+1) - 2m_\chi^2) \\
& + a_\chi^2(2x^2-2x+1)(m_t'^2 + 2m_\chi^2)) \\
& + (b_\chi^2(m_t'^2(1-2x)^2 - 2m_\chi^2(6x^2-6x+1)) \\
& + a_\chi^2(1-2x)(m_t'^2 + 2m_\chi^2))],
\end{aligned}
\tag{A10}
$$

$$
\begin{aligned}
f_8 = {} & -\frac{g_s^2 g_t^2}{192 m_\chi x(x-1)(m_t'^2 - m_V^2)^3} \\
& \times[[b_\chi^2(m_t'^4(6x^2-6x+1)(m_V^2 - 6m_\chi^2) \\
& + m_t'^2(2m_V^2 m_\chi^2(22x^2-22x+5) \\
& - 3m_V^4(1-x)^2) + 2m_V^4 x(x-1)(m_V^2 - 4m_\chi^2)) \\
& + a_\chi^2(m_V^2 + 2m_\chi^2)(m_t'^4(6x^2-6x+1) \\
& - 3m_t'^2 m_V^2(1-2x)^2 + 2m_V^4 x(x-1))] \\
& + [a_\chi^2(-2m_t'^4(2x^2-2x+1)(m_V^2 - 6m_\chi^2) \\
& + m_t'^2(m_V^4(-4x^2+4x+1) - 2m_V^2 m_\chi^2(2x^2-2x+7)) \\
& + 2m_V^2 x(x-1)(m_V^2 - 4m_\chi^2)) \\
& + a_t^2(3m_t'^4 - m_V^2)(m_V^2 + 2m_\chi^2) \\
& \times(m_t'^2(2x^2-2x+1) + 2m_V^2 x(x-1))]],
\end{aligned}
\tag{A11}
$$

$$
\begin{aligned}
f_9 = {} & -\frac{g_s^2 g_t^2 m_t'^2}{192 m_\chi x(x-1)(m_t'^2 - m_V^2)^3} \\
& \times[[b_\chi^2(m_t'^4(1-2x)^2 - m_t'^2 \\
& \times(m_V^2(12x^2-12x+5) + 2m_\chi^2(14x^2-14x+1)) \\
& + 2m_V^2 m_\chi^2(14x^2-14x+5)) + b_\chi^2(m_t'^4(1-2x)^2 - m_t'^2 \\
& \times(m_V^2(12x^2-12x+5) + 2m_\chi^2) \\
& - 2m_V^2 m_\chi^2(8x^2-8x+3))] + [b_\chi^2(m_t'^4 \\
& \times(8x^2 - x^2 + 3) + m_t'^2(m_V^2(8x^2-8x+1) \\
& - 2m_\chi^2(34x^2-34x+1)) + 2m_V^2 m_\chi^2(10x^2-10x+7)) \\
& + b_t^2(m_t'^4(8x^2-8x+3) \\
& + m_t'^2(m_V^2(8x^2-8x+1) + 2m_\chi^2(16x^2-16x+5)) \\
& - 2m_V^2 m_\chi^2)]],
\end{aligned}
\tag{A12}
$$

$$
\begin{aligned}
f_{10} = {} & \frac{g_s^2 g_t^2 m_t'^4(a_\chi^2 + b_\chi^2)}{192 m_\chi x(x-1)(m_t'^2 - m_V^2)^2} \\
& \times(6x^2-6x+2).
\end{aligned}
\tag{A13}
$$

References

[1] Bertone G, Hooper D and Silk J 2005 Particle dark matter: evidence, candidates and constraints *Phys. Rept.* **405** 279–390

[2] Drees M and Gerbier G 2012 Mini-Review of Dark Matter: 2012 arXiv:1204.2373

[3] Clowe D, Bradac M, Gonzalez A H, Markevitch M, Randall S W, Jones C and Zaritsky D 2006 A direct empirical proof of the existence of dark matter *Astrophys. J. Lett.* **648** L109–13

[4] Madhavacheril M S, Sehgal N and Slatyer T R 2014 Current dark matter annihilation constraints from CMB and low-redshift data *Phys. Rev.* D **89** 103508

[5] Arcadi G, Dutra M, Ghosh P, Lindner M, Mambrini Y, Pierre M, Profumo S and Queiroz F S 2018 The waning of the WIMP? A review of models, searches, and constraints *Eur. Phys. J.* C **78** 203

[6] Feng J L and Kumar J 2008 The WIMPless miracle: dark-matter particles without weak-scale masses or weak interactions *Phys. Rev. Lett.* **101** 231301

[7] Steigman G, Dasgupta B and Beacom J F 2012 Precise relic WIMP abundance and its impact on searches for dark matter annihilation *Phys. Rev.* D **86** 023506

[8] Hochberg Y, Kuflik E, Volansky T and Wacker J G 2014 Mechanism for thermal relic dark matter of strongly interacting massive particles *Phys. Rev. Lett.* **113** 171301

[9] Lin T 2019 Dark matter models and direct detection *PoS* **333** 009

[10] Dvali G, Gruzinov A and Zaldarriaga M 2004 Cosmological perturbations from inhomogeneous reheating, freezeout, and mass domination *Phys. Rev.* D **69** 083505

[11] Tanabashi M *et al* 2018 Review of particle physics *Phys. Rev.* D **98** 030001

[12] Miransky V A, Tanabashi M and Yamawaki K 1989 Dynamical electroweak symmetry breaking with large anomalous dimension and t quark condensate *Phys. Lett.* B **221** 177–83

[13] Tait T M P and Yuan C P 2000 Single top quark production as a window to physics beyond the standard model *Phys. Rev.* D **63** 014018

[14] Cheung K, Mawatari K, Senaha E, Tseng P-Y and Yuan T-C 2010 The top window for dark matter *J. High Energy Phys.* JHEP10(2010)081

[15] Zhang Y 2013 Top quark mediated dark matter *Phys. Lett.* B **720** 137–41

[16] Cornell A S, Deandrea A, Flacke T, Fuks B and Mason L 2021 Contact interactions and top-philic scalar dark matter *J. High Energy Phys.* JHEP07(2021)026

[17] Lin T, Kolb E W and Wang L-T 2013 Probing dark matter couplings to top and bottom quarks at the LHC *Phys. Rev.* D **88** 063510

[18] Haisch U and Re E 2015 Simplified dark matter top-quark interactions at the LHC *J. High Energy Phys.* JHEP06 (2015)078

[19] Arina C *et al* 2016 A comprehensive approach to dark matter studies: exploration of simplified top-philic models *J. High Energy Phys.* JHEP11(2016)111

[20] Haisch U and Polesello G 2019 Searching for production of dark matter in association with top quarks at the LHC *J. High Energy Phys.* JHEP02(2019)029

[21] D'Hondt J, Mariotti A, Mawatari K, Moortgat S, Tziveloglou P and Van Onsem G 2016 Signatures of top flavour-changing dark matter *J. High Energy Phys.* JHEP03 (2016)060

[22] Cox P, Medina A D, Ray T S and Spray A 2016 Novel collider and dark matter phenomenology of a top-philic Z' *J. High Energy Phys.* JHEP06(2016)110

[23] An H, Wang L-T and Zhang H 2014 Dark matter with t-channel mediator: a simple step beyond contact interaction *Phys. Rev.* D **89** 115014

[24] Baek S, Ko P and Wu P 2016 Top-philic scalar dark matter with a vector-like fermionic top partner *J. High Energy Phys.* JHEP10(2016)117

[25] Baek S, Ko P and Wu P 2018 Heavy quark-philic scalar dark matter with a vector-like fermion portal *J. Cosmol. Astropart. Phys.* JCAP07(2018)008

[26] Arina C 2018 Impact of cosmological and astrophysical constraints on dark matter simplified models *Front. Astron. Space Sci.* **5** 30

[27] Colucci S, Fuks B, Giacchino F, Lopez Honorez L, Tytgat M H G and Vandecasteele J 2018 Top-philic vector-like portal to scalar dark matter *Phys. Rev.* D **98** 035002

[28] Colucci S, Giacchino F, Tytgat M H G and Vandecasteele J 2018 Radiative corrections to vectorlike portal dark matter *Phys. Rev.* D **98** 115029

[29] Arina C, Fuks B and Mantani L 2020 A universal framework for t-channel dark matter models *Eur. Phys. J.* C **80** 409

[30] Batell B, Lin T and Wang L-T 2014 Flavored Dark Matter and R-Parity Violation *J. High Energy Phys.* JHEP01(2014)075

[31] Kumar A and Tulin S 2013 Top-flavored dark matter and the forward-backward asymmetry *Phys. Rev.* D **87** 095006

[32] Gomez M A, Jackson C B and Shaughnessy G 2014 Dark matter on top *J. Cosmol. Astropart. Phys.* JCAP12(2014)025

[33] Kilic C, Klimek M D and Yu J-H 2015 Signatures of top flavored dark matter *Phys. Rev.* D **91** 054036

[34] Langacker P 2009 The physics of heavy Z' gauge bosons *Rev. Mod. Phys.* **81** 1199–228

[35] Del Aguila F 1994 The physics of z-prime bosons *Acta Phys. Polon.* B **25** 1317–36

[36] Cvetic M and Godfrey S 1995 Discovery and identification of extra gauge bosons *Electroweak Symmetry Breaking and New Physics at the TeV Scale* (*Advanced Series on Directions in High Energy Physics*) 16 (Singapore: World Scientific) 383–415

[37] Cvetic M and Langacker P 1998 Z' physics and supersymmetry *Adv. Ser. Direct. High Energy Phys.* **18** 312–31

[38] Leike A 1999 The phenomenology of extra neutral gauge bosons *Phys. Rept.* **317** 143–250

[39] Robinett R W and Rosner J L 1982 Prospects for a second neutral vector boson at low mass in SO(10) *Phys. Rev.* D **25** 3036 [Erratum: Phys.Rev.D 27, 679 (1983)]

[40] Hewett J L and Rizzo T G 1989 Low-energy phenomenology of superstring-inspired e6 models *Phys. Rep.* **183** 193–381

[41] Faraggi A E and Nanopoulos D V 1991 A superstring Z' AT O (1-TeV)? *Mod. Phys. Lett.* A **6** 61–8

[42] Faraggi A E 1993 Yukawa couplings in superstring derived standard like models *Phys. Rev.* D **47** 5021–8

[43] Kors B and Nath P 2004 A Stueckelberg extension of the standard model *Phys. Lett.* B **586** 366–72

[44] Feldman D, Liu Z and Nath P 2006 The stueckelberg Z prime at the LHC: discovery potential, signature spaces and model discrimination *J. High Energy Phys.* JHEP11(2006)007

[45] Jackson C B, Servant G, Shaughnessy G, Tait T M P and Taoso M 2010 Higgs in space! *J. Cosmol. Astropart. Phys.* JCAP04(2010)004

[46] Jackson C B, Servant G, Shaughnessy G, Tait T M P and Taoso M 2013 Gamma rays from top-mediated dark matter annihilations *J. Cosmol. Astropart. Phys.* JCAP07(2013)006

[47] Di Chiara S, Keus V and Lebedev O 2015 Stabilizing the Higgs potential with a Z' *Phys. Lett.* B **744** 59–66

[48] Greiner N, Kong K, Park J-C, Park S C and Winter J-C 2015 Model-independent production of a top-philic resonance at the LHC *J. High Energy Phys.* JHEP04(2015)029

[49] Darmé L, Fuks B and Maltoni F 2021 Top-philic heavy resonances in four-top final states and their EFT interpretation *J. High Energy Phys.* JHEP09(2021)143

[50] Cao Q-H, Fu J-N, Liu Y, Wang X-H and Zhang R 2021 Probing top-philic new physics via four-top-quark production *Chin. Phys.* C **45** 093107

[51] Aad G *et al* 2024 Search for top-philic heavy resonances in pp collisions at $\sqrt{s} = 13$ TeV with the ATLAS detector *Eur. Phys. J.* C **84** 157

[52] Kundu A 1996 Electroweak precision data and a heavy z-prime *Phys. Lett.* B **370** 135–40

[53] Erler J, Langacker P, Munir S and Rojas E 2009 Improved constraints on z-prime bosons from electroweak precision data *J. High Energy Phys.* JHEP08(2009)017

[54] Bélanger G, Boudjema F, Pukhov A and Semenov A 2015 micrOMEGAs4.1: two dark matter candidates *Comput. Phys. Commun.* **192** 322–9

[55] Fuks B 2019 Cornering top-philic dark matter with colliders and cosmology: the importance of QCD corrections *J. Phys. Conf. Ser.* **1271** 012017

[56] Khachatryan V *et al* 2016 Search for anomalous single top quark production in association with a photon in pp collisions at $\sqrt{s} = 8$ TeV *J. High Energy Phys.* JHEP04 (2016)035

[57] Khachatryan V *et al* 2017 Search for anomalous Wtb couplings and flavour-changing neutral currents in t-channel single top quark production in pp collisions at $\sqrt{s} = 7$ and 8 TeV *J. High Energy Phys.* JHEP02(2017)028

[58] Aad G *et al* 2016 Search for single top-quark production via flavour-changing neutral currents at 8 TeV with the ATLAS detector *Eur. Phys. J.* C **76** 55

[59] Sirunyan A M *et al* 2017 Search for associated production of a Z boson with a single top quark and for tZ flavour-changing interactions in pp collisions at $\sqrt{s} = 8$ TeV *J. High Energy Phys.* JHEP07(2017)003

[60] Sirunyan A M *et al* 2018 Search for the flavor-changing neutral current interactions of the top quark and the Higgs boson which decays into a pair of b quarks at $\sqrt{s} = 13$ TeV *J. High Energy Phys.* JHEP06(2018)102

[61] Khachatryan V *et al* 2017 Search for top quark decays via Higgs-boson-mediated flavor-changing neutral currents in

pp collisions at $\sqrt{s} = 8$ TeV *J. High Energy Phys.* JHEP02 (2017)079
[62] Glashow S L and Weinberg S 1977 Natural conservation laws for neutral currents *Phys. Rev.* D **15** 1958
[63] Freytsis M and Ligeti Z 2011 On dark matter models with uniquely spin-dependent detection possibilities *Phys. Rev.* D **83** 115009
[64] Jacob M and Wick G C 1959 On the general theory of collisions for particles with spin *Annals Phys.* **7** 404–28 [Annals Phys.281,774(2000)]
[65] Cirelli M, Fornengo N and Strumia A 2006 Minimal dark matter *Nucl. Phys.* B **753** 178–94
[66] Essig R 2008 Direct detection of non-chiral dark matter *Phys. Rev.* D **78** 015004
[67] Belanger G, Boudjema F, Pukhov A and Semenov A 2009 Dark matter direct detection rate in a generic model with micrOMEGAs 2.2 *Comput. Phys. Commun.* **180** 747–67
[68] Abe T and Sato R 2015 Quantum corrections to the spin-independent cross section of the inert doublet dark matter *J. High Energy Phys.* JHEP03(2015)109
[69] Hill R J and Solon M P 2015 Standard model anatomy of WIMP dark matter direct detection II: QCD analysis and hadronic matrix elements *Phys. Rev.* D **91** 043505
[70] Dulat S, Hou T-J, Gao J, Guzzi M, Huston J, Nadolsky P, Pumplin J, Schmidt C, Stump D and Yuan C P 2016 New parton distribution functions from a global analysis of quantum chromodynamics *Phys. Rev.* D **93** 033006
[71] Hisano J, Ishiwata K and Nagata N 2010 Gluon contribution to the dark matter direct detection *Phys. Rev.* D **82** 115007
[72] Hill R J and Solon M P 2015 Standard model anatomy of WIMP dark matter direct detection I: weak-scale matching *Phys. Rev.* D **91** 043504
[73] Novikov V A, Shifman M A, Vainshtein A I and Zakharov V I 1984 Calculations in external fields in quantum chromodynamics. Technical review *Fortsch. Phys.* **32** 585
[74] Mohan K A, Sengupta D, Tait T M P, Yan B and Yuan C P 2019 Direct detection and LHC constraints on a t-channel simplified model of majorana dark matter at one loop *J. High Energy Phys.* JHEP05(2019)115
[75] Passarino G and Veltman M J G 1979 One loop corrections for e + e- annihilation into mu+ mu- in the Weinberg model *Nucl. Phys.* B **160** 151–207
[76] 't Hooft G and Veltman M J G 1979 Scalar one loop integrals *Nucl. Phys.* B **153** 365–401
[77] Meng Y *et al* 2021 Dark matter search results from the PandaX-4T commissioning run *Phys. Rev. Lett.* **127** 261802
[78] Aalbers J *et al* 2023 A next-generation liquid xenon observatory for dark matter and neutrino physics. *J. Phys.* G **50** 013001